J Mater Sci: Mater Electron (2016) 27:474–480
DOI 10.1007/s10854-015-3776-7

Novel silver-doped $CdMoO_4$: synthesis, characterization, and its photocatalytic performance for methyl orange degradation through the sonochemical method

S. Mostafa Hosseinpour-Mashkani[1] · Mahnaz Maddahfar[1] · Ali Sobhani-Nasab[1]

Received: 12 August 2015 / Accepted: 12 September 2015 / Published online: 12 October 2015

Abstract A novel silver-doped tetragonal phase of cadmium molybdate nanoparticles (Ag°–$CdMoO_4$) were successfully synthesized through the sonochemical method. The effect of processing parameters such as the dosage of sucrose and ultrasonic power on the morphology and particle size was investigated. Furthermore, sucrose was applied as a green capping agent. The sample indicated a ferromagnetic behavior, as evidenced by using vibrating sample magnetometer (VSM) at room temperature. The SEM results revealed that the morphology of $CdMoO_4$ nanoparticles is highly dependent on the reaction conditions. Photocatalytic activities of the Ag°–$CdMoO_4$ samples were evaluated by the degradation of methyl orange dye under visible light irradiation. It has been observed that the sample containing 0.5 mol of Ag showed the best photocatalytic activity as compared to other samples. The nanoparticles structure has been elucidated by XRD, SEM, UV–Vis, EDX, VSM, and FTIR.

1 Introduction

Nanoparticles have gained much attention among materials, because the nanocrystal properties not only depend on their composition but also depend on their size, shape, and size distribution [1–7]. Photocatalytic degradation of organic compounds on semiconductor surface has attracted increasing attention in recent years because the technique is regarded as one of the most promising and efficient solution for the removal of organic pollutants [8–12]. The scheelite structured ternary compounds such as molybdates of Pb^{2+}, Ca^{2+}, and Cd^{2+}, which belong to the molybdate family, have been studied in the past as potential materials for photoluminescence, solid state lasers, optical fibers, scintillating materials, magnetic materials, sensor materials, etc. [13–15]. Recent researches have shown that some of these tungstate family compounds such as $CaMoO_4$, $PbMoO_4$, and $CdMoO_4$ show their attractive photocatalytic activity for the degradation of organic pol-lutants despite of their relatively larger band-gap energies [16]. However, very few studies have been found on $CdMoO_4$ as a photocatalytic material for the degradation of organic pollutants [17–20]. It has been reported in literatures that heterojunction in photocatalysis provides an easy steps for harvesting light energy for those materials which have relatively larger energy band gap and thus make it visible light active photocatalyst. Despite this, reducing the chances of recombination of electron-hole pairs formed during photo-electron excitation is another decisive factor to improve efficiency of heterogeneous photocatalysis. Several synthesis routes have already been proposed in the past for the synthesis of $CdMoO_4$ including chemical precipitation, hydrothermal/solvothermal, microwave, etc. and evaluation of photocatalytic activity for the degradation of organic pollutants under UV light irradiation [21, 22]. We tried to extend our knowledge to apply the sonochemical technique to synthesize $CdMoO_4$ photo-catalyst. The physical phenomenon responsible for the ultrasonic process is acoustic cavitation. The ultrasonic cavitation generates a very strong stirring environment. Therefore, application of ultrasound is expanding in material science for dispersion, emulsifying, crushing, impregnation, surface treatment, synthesis and activation of nanoparticles. During the process, the rapid ultrasonic vibrations and cavitation effects cause to increase collision between the molecules which in turn enhance the chemical reactivity [23–27]. In the current study, the synthesis of

✉ Ali Sobhani-Nasab
Ali.sobhaninasab@gmail.com

[1] Young Researchers and Elites Club, Arak Branch, Islamic Azad University, Arak, Iran

Table 1 Reaction conditions for $CdMoO_4$ nanoparticles

Sample nos.	Power (W)	Capping agent	Ag-dope	Decolorization (%)
1	50	–	–	–
2	50	Sucrose	–	–
3	70	–	–	40
4	70	Sucrose	–	–
5	90	–	–	–
6	90	Sucrose	–	–
7	70	–	0.3	75
8	70	–	0.5	98

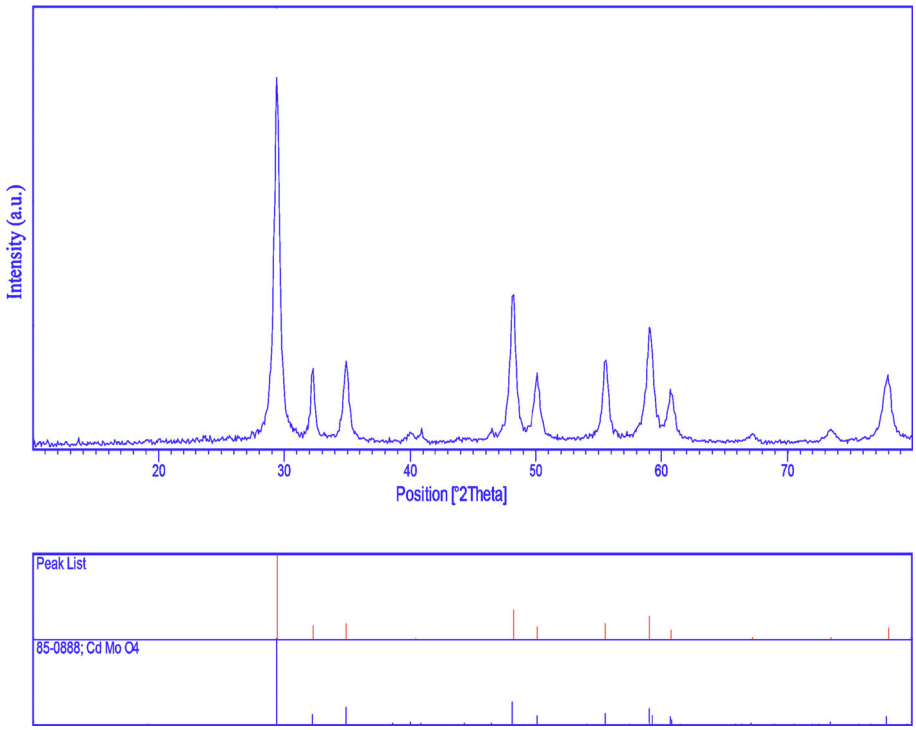

Fig. 1 XRD pattern of $CdMoO_4$ nanoparticles (sample no 3)

$CdMoO_4$ nanoparticles is reported. This production is done by ultrasonic solution of cadmium (II) nitrate hexahydrate and ammonium molybdate tetrahydrate. Besides, the effect of reaction parameters such as dosage of sucrose and ultrasonic power on the morphology and particle size of $CdMoO_4$ nanoparticles was investigated. Furthermore, the as-synthesized $CdMoO_4$ was used as an efficient photocatalyst for the photocatalytic degradation of methyl orange (MO) dye within 120 min.

2 Experimental

2.1 Materials and chacterization

All chemical reagents in this experiment were of analytical grade and used without further purification. X-ray diffraction (XRD) patterns were recorded by a Philips-X'PertPro, X-ray diffractometer using Ni-filtered Cu Kα radiation at scan range of $10 < 2\theta < 80$. Scanning electron microscopy (SEM) images were obtained on LEO-1455VP equipped with an energy dispersive X-ray spectroscopy. Fourier transform infrared (FT-IR) spectra were recorded on Magna-IR, spectrometer 550 Nicolet with 0.125 cm^{-1} resolution in KBr pellets in the range of 400–4000 cm^{-1}. UV–Vis diffuse reflectance spectroscopy analysis (UV–Vis) was carried out using Shimadzu UV–Vis scanning spectrometer. Ultrasonic irradiation was accomplished with a high-intensity ultrasonic bath. The EDS analysis with 20 kV accelerated voltage was done. The magnetic measurement of sample was carried out in a vibrating sample magnetometer (VSM) (Meghnatis Daghigh Kavir Co.; Kashan Kavir; Iran) at room temperature.

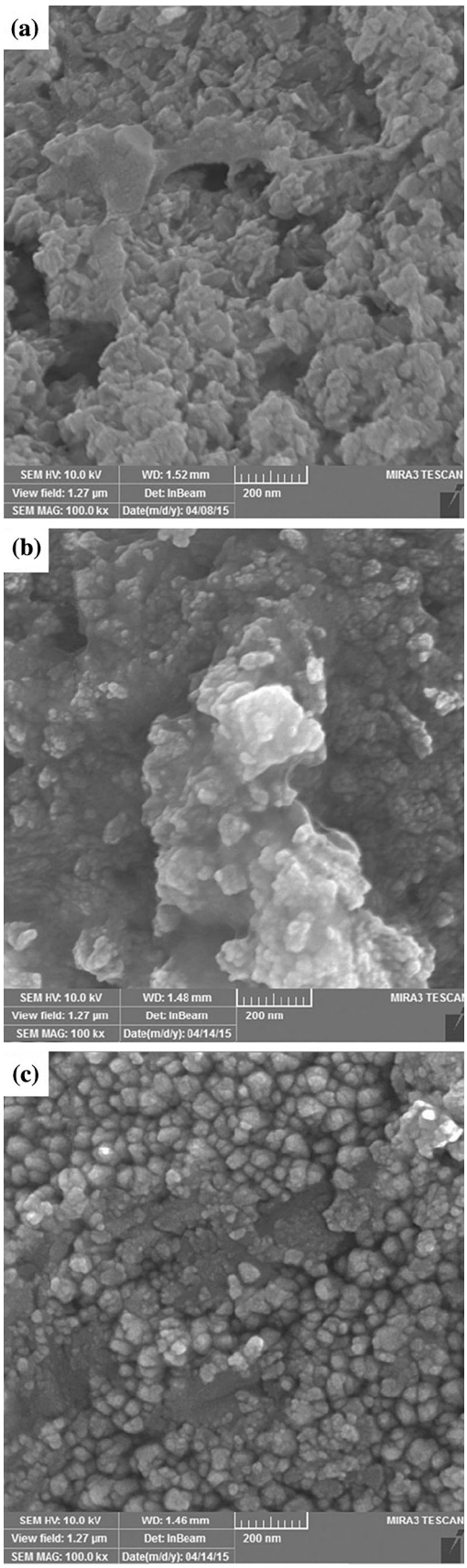

◀**Fig. 2** SEM images of $CdMoO_4$ nanoparticles **a** sample no 1 **b** sample no 3 **c** sample no 5

2.2 Synthesis of $CdMoO_4$ nanoparticles

$Cd(NO_3)_3{\cdot}6H_2O$ (0.101 g) and $(NH_4)_6Mo_7O_{24}{\cdot}4H_2O$ (0.058 g) was dissolved in 60 ml of distilled water separately. Then, 0.224 g of sucrose as natural surfactant was added to the $Cd(NO_3)_3{\cdot}6H_2O$ solution and loaded into a beaker; the reaction was carried out in an ultrasonic digestion system at 70 W for 30 min. Subsequently, during the sonication, the solution of $(NH_4)_6Mo_7O_{24}{\cdot}4H_2O$ was added into the above solution. After irradiation, the system was allowed to cool to room temperature naturally, the obtained precipitate was collected by filtration, and washed with absolute ethanol and distilled water several times. Finally, the product was dried in vacuum at 90 °C for 2 h. Reaction conditions are listed in Table 1.

2.3 Synthesis of Ag°–$CdMoO_4$ nanoparticles

The stoichiometric ratios of $CdMoO_4$ (samples 3, 1 mmol) and $AgNO_3$ (0.3 and 0.5 mmol) were dissolved in 30 ml of distilled water under magnetic stirring to form a homogeneous solution. Then, a solution contains hydrazine monohydrate (N_2H_4) as a reduction was added drop wise to the above mention solution. Subsequently, the system was allowed to cool to room temperature naturally, the obtained precipitate was collected by filtration, then washed with absolute ethanol, and distilled water several times. Finally, the product was dried in vacuum at 80 °C for 1 h.

2.4 Photocatalytic experimental

In order to evaluate photocatalytic activity of the samples 3, 7, and 8, catalytic decolorization of methyl orange dyes under visible light irradiation were performed at room temperature. In a typical experiment, 100 mg of samples 3, 7, and 8 were added into a glass beaker containing 50 ml of dye aqueous solution (5 mg/l), and then dispersed by stirring for 30 min at darkness to establish adsorption–desorption equilibrium between the dye molecules and catalyst surface. The photocatalytic experiments were performed under an irradiation wavelength of $\lambda > 400$ nm. The photocatalytic activities of nanocrystalline cadmium molybdate obtained from samples no. 3, 7, and 8 were studied by the degradation of methyl orange solution as a target pollutant. Later, the mixture was placed inside the photoreactor in which the

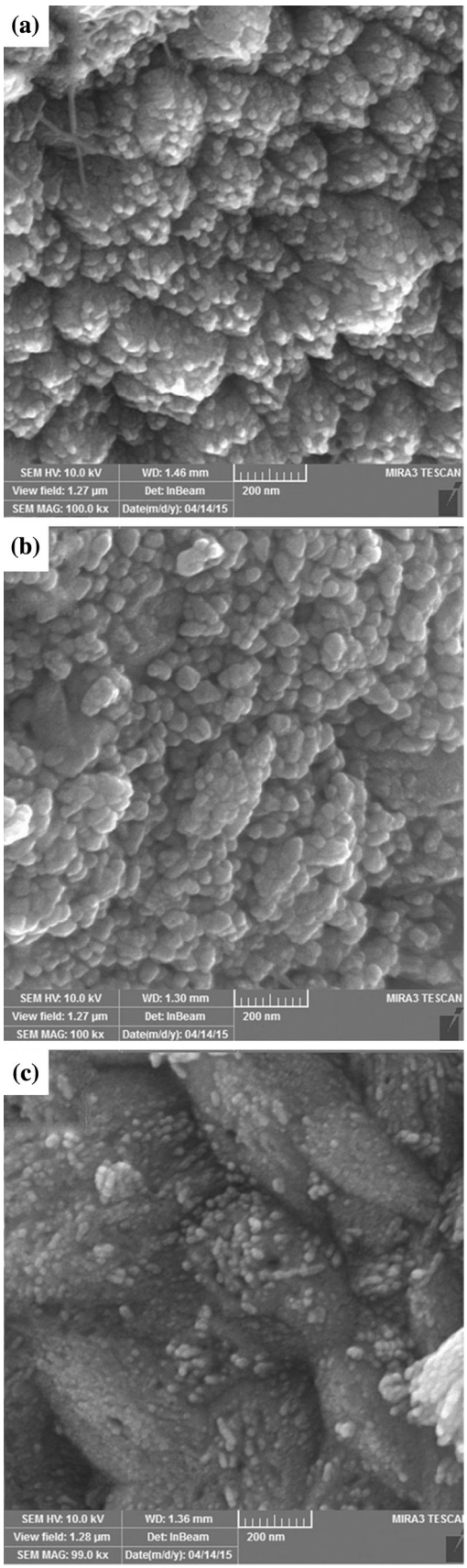

◀**Fig. 3** SEM images of $CdMoO_4$ nanoparticles **a** sample no 2 **b** sample no 4 **c** sample no 6

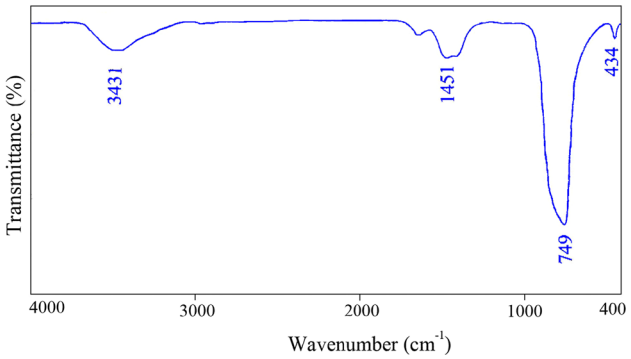

Fig. 4 FT-IR spectrum of $CdMoO_4$ nanoparticles (sample no 3)

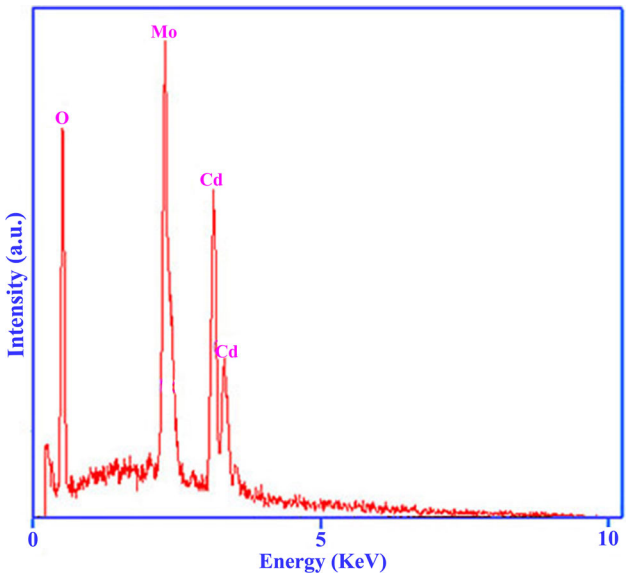

Fig. 5 EDS pattern of $CdMoO_4$ nanoparticles (sample no 3)

vessel was 15 cm away from the visible source of 400 W Xeno lamp. Aliquots of the mixture were taken at definite interval of times during the irradiation, and after centrifugation they were analyzed by a UV–Vis spectrometer.

3 Results and discussion

Figure 1 shows a typical XRD pattern ($10° < 2\theta < 80°$) of $CdMoO_4$ nanoparticles (sample 3). Based on the Fig. 1, the diffraction peaks can be indexed to pure tetragonal phase of $CdMoO_4$ (space group *I41/a*, JCPDS No. 85-0888). No other crystalline phases were detected. From XRD data, the crystallite diameter (D_c) of $CdMoO_4$ nanoparticles

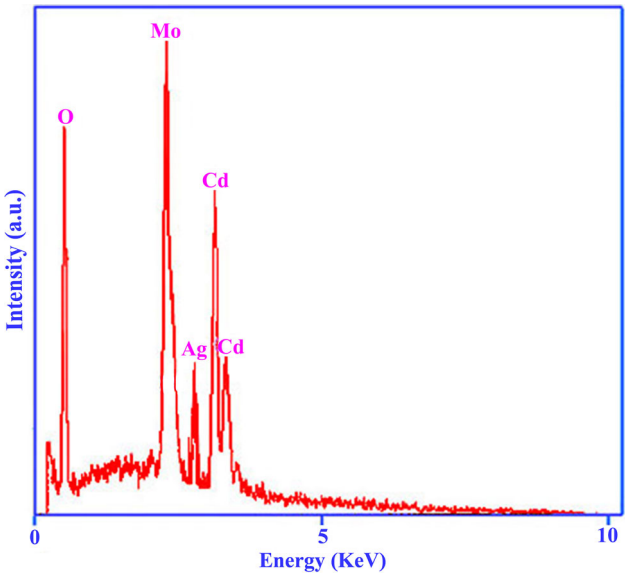

Fig. 6 EDS pattern of Ag–$CdMoO_4$ nanoparticles (sample no 3)

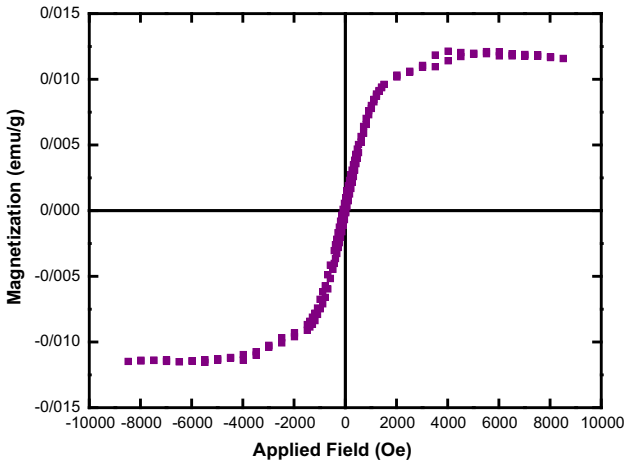

Fig. 7 VSM curves of $CdMoO_4$ nanoparticles (sample no 3)

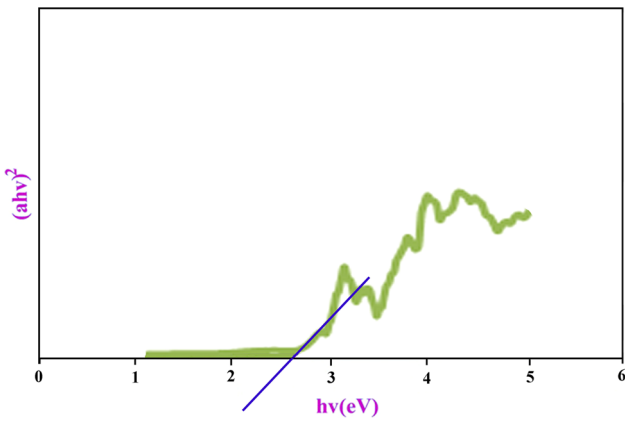

Fig. 8 UV–Vis pattern of $CdMoO_4$ nanoparticles (sample no 3)

obtained from sample 3 was calculated to be 35 nm using the Scherer equation:

$$D_c = K\lambda/\beta\cos\theta \qquad \text{Scherer equation}$$

where β is the breadth of the observed diffraction line at its half intensity maximum, K is the so-called shape factor, which usually takes a value of about 0.9, and λ is the wavelength of X-ray source used in XRD. The effects of different dosage of sucrose and ultrasonic power on the morphology and particle size of final products were investigated. To investigate the effect of ultrasonic powers on the morphology and particle size of $CdMoO_4$ three experiments were performed (Fig. 2a, b, c, samples no 1, 3, and 5 respectively). Base on the Fig. 2a, the product is mainly composed of the agglomeration nanoparticles. When ultrasonic power increased from 50 to 70 W, morphology of $CdMoO_4$ is consist of nanoparticle with average particle size 50–70 nm, as shown in Fig. 2b. Expanding the ultrasonic power from 70 (sample 3) to 90 W (sample 5) causes increase the particle size of products, as shown in Fig. 2c. As a result, increase ultrasonic power causes decrease particles size of products and agglomeration of final products. Sucrose was used as capping agent at the same ultrasonic powers to show its effect on the morphology and particle size of final products (Fig. 3a, b, c, samples no 2, 4, and 6 respectively). According to the Fig. 3a, b, c, product is mainly consists of agglomeration nanoparticles. Compared with samples no 1, 3, and 5, add sucrose as capping agent has resulted in agglomeration nanoparticles. Therefore, optimum condition for synthesis $CdMoO_4$ is sample 3. The FT-IR spectrum of $CdMoO_4$ nanoparticles (sample 3) in the range 400–4000 cm^{-1} is shown in Fig. 4. The absorption bond at 3431 and 1627 cm^{-1} are attributable to the v(OH) stretching and bending vibrations, respectively, which indicates the presence of physisorbed water molecules linked to $CdMoO_4$ nanoparticles [28]. The peak at 749 cm^{-1} is assigned to vibrations of the Mo–O–Mo. Furthermore, the absorption peak at 434 cm^{-1} is assigned to ν_3 vibration of the same group [29].

The EDS analysis measurement was used to investigate the chemical composition and purity of $CdMoO_4$ nanoparticles (sample 3, Fig. 5). According to the Fig. 5, the product consists of Cd, Mo, and O elements. Furthermore, neither N nor C signals were detected in the EDS spectrum, which means the product is pure and free of any surfactant or impurity. EDS spectrum of Ag-0.3 $CdMoO_4$ (sample 7, Fig. 6) shows the Cd, Mo, O, and Ag elements which confirms the presence of Ag in the final products. The VSM magnetic measurements for the $CdMoO_4$ Fig. 7 show the magnetic properties of nanoparticles prepared at low temperature. The nanoparticles exhibit ferromagnetic behaviour at room temperature, with a saturation

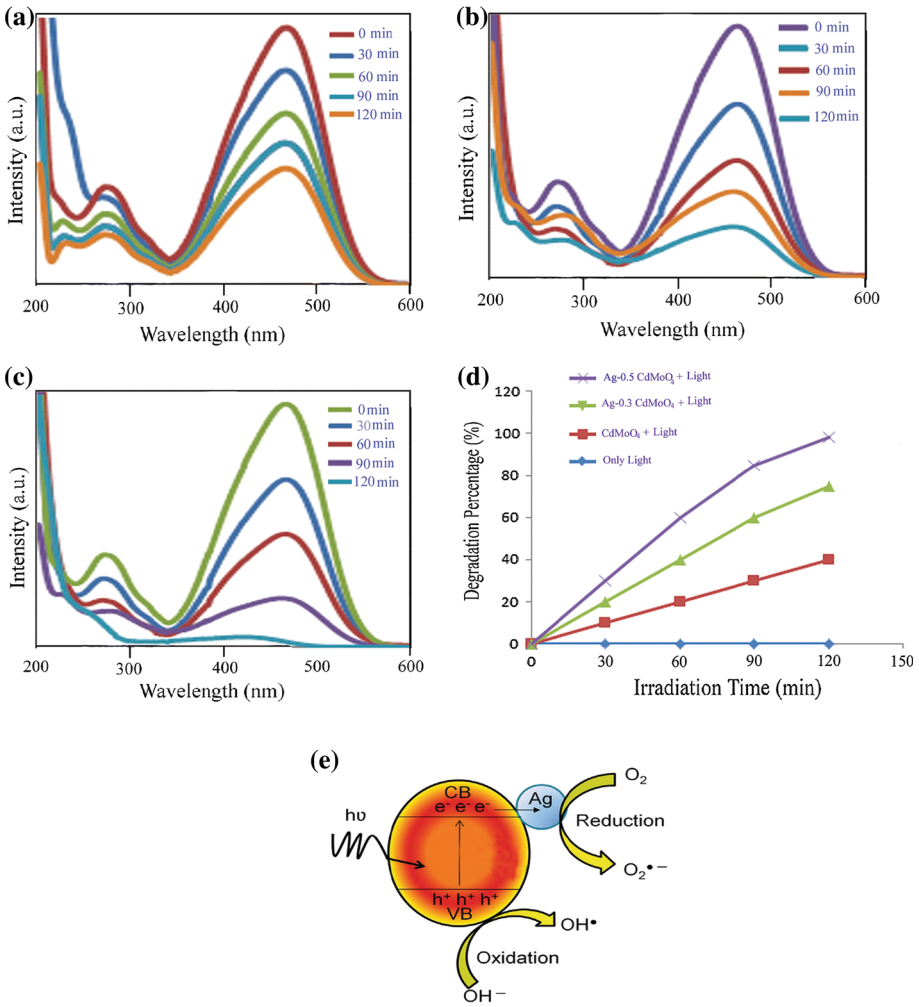

Fig. 9 **a–c** fluorescence spectral time scan of methyl orange in the presence of samples 3, 7, and 8 **d** photocatalytic methyl orange degradation of samples 3, 7, and 8 under visible light and (**d**) reaction mechanism of methyl orange photodegradation under visible light irradiation

magnetization of 0.011 emu/g and a coercivity of 50 Oe. To investigate the optical properties of the $CdMoO_4$, UV–Vis spectrum was recorded. Figure 8 shows the UV–Vis diffuse reflectance spectrum of $CdMoO_4$ nanoparticles (sample 3). Using Tauc's formula, the band gap can be obtained from the absorption data. The energy gap (Eg) of the nanocrystalline $CdMoO_4$ has been estimated by extrapolating the linear portion of the plot of $(\alpha h\nu)^2$ against hν to the energy axis. The Eg value of the nanocrystalline $CdMoO_4$ calculated to be 2.9 eV. For studying the photocatalytic properties of the as-prepared nanoparticles, the photodegradation of methyl orange was employed as typical models of organic dyes. In this order, the decolorization of dye was measured by the diminution of its absorption as a function of the visible light irradiation time. Figure 9a, b and c exhibit the removal rates of methyl orange, from aqueous solution under visible light illumination in the presence of samples 3, 7, and 8. The decolorization efficiency (%) was calculated by the following equation, where A_0 is the initial absorption of the dye solution and A is its absorption at appropriate time (120 min).

$$\text{Decolorization } \% = 100\,(A_0 - A)/A_0 \quad (1)$$

The absorbance intensities of methyl orange are gradually decreased in the presence of samples 3, 7, and 8 with the increase of exposed time, indicating a decrease in dye concentration. From the graphs (Fig. 9 a, b, c), it is clear that in the presence of samples 3, 7, and 8 as a photocatalyst, it is estimated that maximum 40, 75, and 98 % of methyl orange is degraded within 120 min under visible light irradiation, respectively. As a result, Ag as a dope causes increase in photocatalytic activity of $CdMoO_4$. The mechanism for the enhanced photocatalysis of Ag/$CdMoO_4$ could be proposed as follow. Under the irradiation, the electrons (e^-_{cb}) are excited from the valence band to the conduction band of $CdMoO_4$ leaving behind h^+_{vb}. Ag^+ doping in $CdMoO_4$ being lewis acid due to the presence of partially filled S-orbital can effectively trap the e^-_{cb} and inhibit the recombination with h^+_{vb}. The reduced state

of Ag^+ ions, with 1S electrons, is very instable so that the e_{cb}^- can be easily detrapped and transferred to the O_2 molecules promoting the $O^{\cdot}{}_2^-$ formation and then converted to active ·OH. This suggested that the Ag dopant can serve as an effective charge carrier trap and facilitated the excited e_{cb}^- transfer under visible light irradiation. The degradation mechanism for the $Ag/CdMoO_4$ can be given as:

$$CdMoO_4 + h\nu \rightarrow e^-(CB) + h^+(VB) \quad (2)$$

$$Ag^+ + e_{cb}^- \rightarrow Ag^{\circ}(\text{electron trapping}) \quad (3)$$

$$Ag + O_2 \rightarrow Ag^+ + O_2^-(\text{electron transfer}) \quad (4)$$

$$O_2^- + H^+ \rightarrow {}^{\cdot}OOH \quad (5)$$

$${}^{\cdot}OOH + H^+ + e_{cb}^- \rightarrow H_2O_2 \quad (6)$$

$$H_2O_2 + e_{cb}^- \rightarrow {}^{\cdot}OH + OH^- \quad (7)$$

At the same time, the photogenerated $h^+{}_{vb}$ can be captured on the catalyst surface undergoing charge transfer with adsorbed water molecules or with surface-bound hydroxide species to generate active ·OH as shown in steps:

$$h_{vb}^+ + H_2O \rightarrow H^+ + {}^{\cdot}OH \quad (8)$$

$$h_{vb}^+ + OH^- \rightarrow {}^{\cdot}OH \quad (9)$$

Thus, the separation of the charge carriers was attributed to such trapping by Ag dopant in $CdMoO_4$. Subsequently, enhanced the yield of ·OH quantities in the degradation of methyl orange, which further improved the photocatalytic activity of $Ag/CdMoO_4$.

4 Conclusions

$CdMoO_4$ nanoparticles have been successfully synthesized through an ultrasonic method. Sucrose was applied as green surfactant agent. Furthermore, we investigated the effect of dosage of sucrose and ultrasonic power on the morphology and particle size of $CdMoO_4$ nanoparticles. SEM results indicated that the size and morphology of the products could were found to be greatly influenced by the aforementioned parameters. $CdMoO_4$ nanoparticles were characterized by XRD, FT-IR, UV–Vis, EDS, and SEM. VSM analyzes indicate a paramagnetic behavior for the synthesized nanoparticles. Moreover, the photocatalyst results reveal that increase in concentration of Ag dope from 0.3 to 0.5 results in increase decolorization of methyl orange from 75 to 98 % in 120 min of stirring under visible light irradiation.

Acknowledgments Authors are grateful to council of University of Arak for providing financial support to undertake this work.

References

1. M. Ramezani, A. Davoodi, A. Malekizad, S.M. Hosseinpour-Mashkani, J. Mater. Sci.: Mater. Electron. **26**, 3957 (2015)
2. M. Zahraei, A. Monshi, D. Shahbazi-Gahrouei, M. Amirnasr, B. Behdadfar, M. Rostami, J. Nanostruct. **5**, 137 (2015)
3. M. Mousavi-Kamazani, M. Salavati-Niasari, D. Ghanbari, J. Nanostruct. **2**, 363 (2012)
4. M. Shahrekizad, A. Gholamalizadeh-Ahangar, N. Mir, J. Nanostruct. **5**, 117 (2015)
5. F. Beshkar, M. Salavati-Niasari, JNS **5**, 17 (2015)
6. M. Panahi-Kalamuei, M. Mousavi-Kamazani, M. Salavati-Niasari, J. Nanostruct. **4**, 459 (2014)
7. N. Asadi, R. Naderi, M. Saremi, F. Deflorian, J. Ultrafine Grained Nanostruct. Mater. **47**, 9 (2014)
8. A. Yousef, N.A.M. Barakat, T. Amna, A.R. Unnithan, S.S. Al-Deyab, H.Y. Kim, J. Lumin. **132**, 1668 (2012)
9. Y. Zhao, L. Kuai, B. Geng, Catal. Sci. Technol. **2**, 1269 (2012)
10. S.X. Liu, Toxicol **74**, 706 (2005)
11. J.C.S. Wu, Catal. Surv. Asia **13**, 30 (2009)
12. A. Kudo, M. Steinberg, A.J. Bard, A. Campion, M.A. Fox, T.E. Mallouk, S.E. Webber, J.M. White, Catal. Lett. **5**, 61 (1990)
13. J. Lin, Z. Zeng, Q. Wang, Inorg. Chim. Acta **408**, 59 (2013)
14. L.R. Hou, L. Lian, L.H. Zhang, J.Y. Li, Mater. Lett. **109**, 306 (2013)
15. Y. Yu-Linga, L. Xue-Minga, F. Wen-Lina, L. Wu-Lina, T. Chuan-Yia, J. Alloys Comp. **505**, 239 (2010)
16. Q.L. Dai, G.G. Zhang, P. Liu, J. Wang, J.K. Tang, Inorg. Chem. **51**, 9232 (2012)
17. D.B. Hernandez-Uresti, C.A. Martinez-de, L.M. Torres-Martinez, Res. Chem. Intermed. **38**, 817 (2012)
18. D. Li, Y.F. Zhu, Cryst. Eng. Comm. **14**, 1128 (2012)
19. H.W. Liu, L. Tan, Ionics **16**, 57 (2010)
20. Y. Shimodaira, H. Kato, H. Kobayashi, A. Kudo, Bull. Chem. Soc. Jpn **80**, 885 (2007)
21. D. Zhu, K. Ki, X. Chen, T. Ying, Adv. Mater. **5**, 403 (2011)
22. A. Phuruangrat, T. Thongtem, S. Thongtem, J. Cryst. Growth **311**, 4076 (2009)
23. S. Anandan, M. Ashokkumar, Ultrason. Sonochem. **16**, 316 (2009)
24. T.H. Kim, V. Rodríguez-González, G. Gyawali, S.H. Cho, T. Sekino, S.W. Lee, Catal. Today **9**, 14 (2012)
25. A.M. Behpour, A.M. Mehrzad, S.M. Hosseinpour-Mashkani, JNS **5**, 183 (2015)
26. M. Riazian, JNS **4**, 433–441 (2014)
27. L.R. Hou, C.Z. Yuan, Y. Peng, J. Hazard. Mater. **139**, 310 (2007)
28. L. Nejati-Moghadam, A. Esmaeili Bafghi-Karimabad, M. Salavati-Niasari, H. Safardoust, J. Nanostruct. **5**, 47 (2015)
29. E. Khosravifard, M. Salavati-Niasari, M. Dadkhah, G. Sodeifian, J. Nanostruct. **2**, 191 (2010)